

# Computational chemistry applied to reactions in electrocatalysis

Axel Groß and Sebastian Schnur  
*Institut für Theoretische Chemie, Universität Ulm,  
Albert-Einstein-Allee 11, 89069 Ulm/Germany  
Email: axel.gross@uni-ulm.de*

In this chapter, the theoretical and computational challenges for a first-principles description of chemical reactions at the solid-liquid interface in the presence of external electric fields and/or varying electrode potentials are reviewed.

## I. INTRODUCTION

In the field of surface science, recent years have witnessed a tremendous progress as far as the microscopic elucidation of structures and processes is concerned [1]. This is not only caused by the development of experimental probes with atomistic resolution, but currently it is also caused to a large extent by advances in theoretical surface science [2]. Due to the ever improving computer power and the development of efficient algorithms a reliable theoretical description of complex surface structures and of processes on surfaces based on first-principles electronic structure theory, in particular density functional theory (DFT) [3], has become possible. DFT methods combine computational efficiency with an acceptable accuracy. Consequently, theoretical studies are no longer limited to explanatory purposes but have gained predictive power. Thus, theory and experiment can collaborate on the same footing, which has resulted in numerous very fruitful collaborations between theoretical and experimental groups addressing surface science problems. One of the many impressive examples is the design of a successful catalyst for the steam-reforming process based on a close collaboration between fundamental academic research, both experimental and theoretical, and industrial development [4].

In electrochemistry and in electrocatalysis, processes do not occur at the solid-gas interface, but rather at the solid-liquid interface. Furthermore, external electric fields are applied leading to varying electrode potentials. This adds considerable complexity to the appropriate theoretical treatment of electrochemical processes at the solid-liquid interface. Furthermore, the number of experimental probes with atomic resolution at the solid-liquid interface is limited compared to the solid-vacuum interface. Consequently, even such elementary properties as the exact structure of water at the electrode-electrolyte interface are still debated. In addition, for seemingly simple reactions such as the hydrogen evolution/oxidation reaction and the oxygen reduction reaction in electrocatalysis relatively little is known about the basic reaction steps [5]. Therefore there is a strong need for theoretical studies leading to a microscopic description and analysis of electrocatalytic reactions.

In fact, there have already been several attempts to model external fields or the electrode potential at the solid-liquid interface within the DFT slab approach [6–

10]. In this chapter, we will try to review the current status of the first-principles treatment of reaction in electrocatalysis including the effect of the electrode potential. We will first give a general introduction into the problems associated with the description of the electrode potential. There are two different approaches to treat charged systems within periodic DFT calculations, either at constant number of electrons or at constant electron chemical potential [6]. Both approaches will be briefly introduced and contrasted. In an electrochemical cell, the potential falls off at the solid/liquid interface within the double layer to a constant value in the electrolyte [11]. The charge on the surface of the electrode is controlled by the potential difference between the metal and the electrolyte and by the capacity of the double layer. Hence it is the potential that is the crucial variable and not the charge so that the calculations should be performed at constant chemical potential rather than constant charge. Yet, calculations at constant charge are usually computationally less demanding.

Furthermore, we will describe DFT studies devoted to the description of the water-metal interaction in the absence of any external fields. Traditionally this was done using parameterized interaction potentials [12], and still the development of water interaction potentials is an active field [13], but nowadays these studies can be performed entirely from first principles [14]. We will in particular focus on the structure of water above late transition metal electrodes.

Finally we will discuss and contrast the different approaches and implementations for modeling external fields and varying electrode potentials. We will give examples of results obtained with the different methods. This is not meant to be an exhaustive overview over recent applications, but rather an illustration of the potential of these methods in elucidating microscopic details of processes in electrocatalysis. In fact, these methods are rather powerful as a means of giving insights into fundamental processes at the electrochemical solid-liquid interface. Still there is no commonly accepted method to describe varying electrode potentials in periodic DFT calculations. All the methods used have advantages, but also some drawbacks. Consequently, it is certainly fair to say that there is still enough room for improvements in the realistic theoretical description of solid-liquid interfaces in the presence of external fields. Nevertheless, it is anticipated that first-principles calculations in elec-

trochemistry will soon play a similar role as in surface science.

## II. THEORETICAL FOUNDATIONS

In order to address extended interface systems from first principles, almost exclusively periodic electronic structure calculations based on density functional theory (DFT) [3] are used. We will first discuss general aspects of DFT calculations related to periodic DFT calculations at the electrochemical solid-liquid interface and then address specific problems related to the treatment of charged systems and to the determination of the electrode potential.

### A. Periodic DFT calculations

Periodic DFT calculations using a plane wave expansion of the one-electron states are computationally rather efficient [15]. Still, at an electrode surface, the three-dimensional periodicity of the bulk system is broken. In order to exploit the efficiency of the periodic DFT codes, a three-dimensional periodicity has to be restored without introducing any artefacts. This is achieved in the so-called supercell approach illustrated in Fig. 1 in which electrodes are represented by repeated slabs of finite thickness that are infinitely extended in lateral directions. Thus the delocalized nature of the electronic states of metal electrodes can be taken into account. The distance between the slabs has to be large enough so that there is no interaction between the electrodes, and the slabs have to be thick enough to give a good representation of the substrates. These conditions can be easily checked by increasing the height of the supercell and the thickness of the slabs, respectively, until convergence of the results of interest with respect to these parameters is reached.

The accuracy of DFT calculations with respect to the quantum many-body effects cannot that easily be assessed. These effects are all included in the exchange-correlation functional which is unfortunately not known so that approximations are needed. Nowadays the generalized gradient approximation (GGA) [16, 17] is typically used in which the gradient of the electron density is taken into account, but in such a way that important sum rules are obeyed. There are still shortcomings of the GGA, for example that van der Waals or dispersion forces are not properly reproduced. However, hydrogen bonds are typically well-described which is rather important for DFT calculations applied to electrochemical systems at the solid-liquid interface.

In periodic DFT calculations addressing surface science problems at the solid-gas or solid-vacuum interface, the space between the slabs is kept empty, but the space between the slabs can equally well be filled up with an electrolyte, as indicated in Fig. 1, so that systems rele-

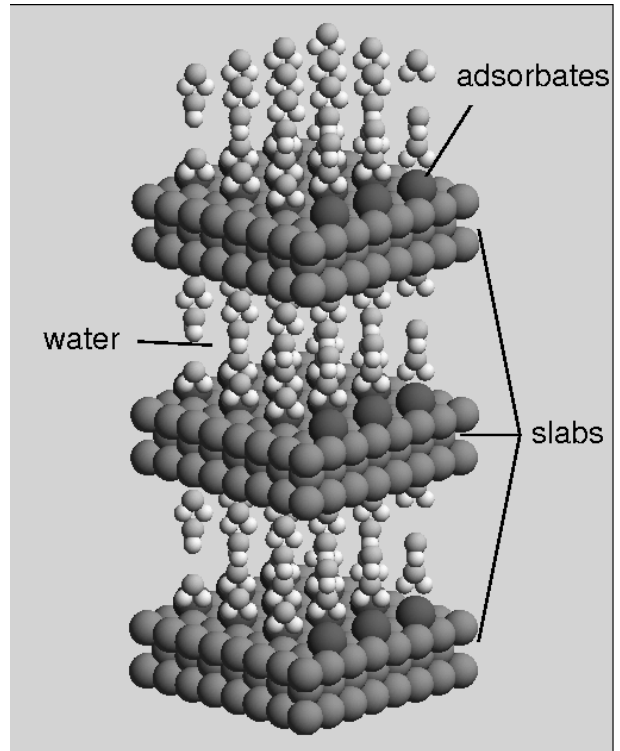


FIG. 1: Illustration of the supercell approach in periodic DFT calculations to describe extended electrode surfaces plus an electrolyte.

vant for electrocatalysis can be addressed. However, for a realistic description of electrochemical system, the presence of external fields which leads to a varying electrode potential has to be modeled as well.

A conceptually easy approach to include electric field effects is to create an external field by introducing a dipole layer in the vacuum region between two slabs representing the surface or interface system [18]. This method was originally developed to correct the dipole field in periodic DFT calculations when the slabs representing the substrate are not symmetric along the surface normal. However, the dipole layer can also be used to deliberately introduce an external field [7]. In this approach, the number of electrons is not changed; thus charge neutrality is also maintained. However, within this approach it is not straightforward to relate the applied dipole field to the corresponding resulting electrode potential.

Charging up the slabs also leads to a variation in the electrode potential. Yet, in periodic calculations the unit cell has to be neutral, i.e., there must not be a net charge per unit cell because otherwise the electrostatical energy diverges. Hence the excess charge has to be balanced by counter charges. These compensating charges can be realized in various ways, for example as a uniform charge background [9], as a localized counter electrode [6] or by the explicit introduction of counter ions [10].

Furthermore, in DFT calculations describing elec-

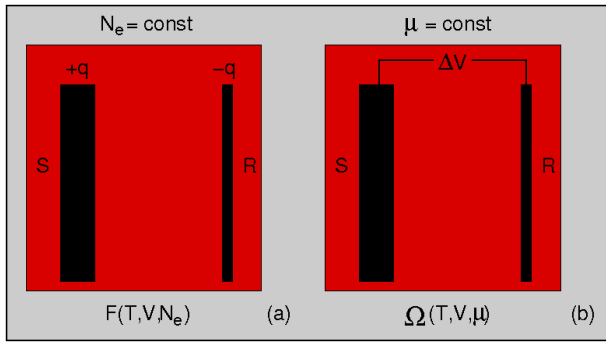


FIG. 2: Illustration of the two possible modes to describe charged systems within DFT: a) constant charge  $N_e = \text{const}$ ; b) constant chemical potential  $\mu = \text{const}$ . The appropriate thermodynamics potentials to treat a slab together with a reference electrode are the Helmholtz free energy  $F$  and the grand potential  $\Omega$ , respectively.

trodes with excess charges, there are in fact two different modes to deal with the charges [6], irrespective of the distribution of the compensating charges. Originally, DFT was formulated for systems with a constant number of electrons  $N_e$ . Very quickly it was realized [19] that there is an equivalent grand canonical formulation of DFT in which the chemical potential  $\mu$  of the electrons instead of the number of electrons is one of the basic quantities.

The differences between these approaches is illustrated in Fig. 2. Systems with a constant number of electrons correspond to an isolated slab placed in an external electric field. This can be realized as a capacitor (Fig. 2a) where the slab and the counter electrode carry charges of equal amount but opposite sign. However, the compensating charge does not need to be locally separated from the charged slab but can also be distributed uniformly over the unit cell as a compensating charge background [9].

The “ $\mu = \text{constant}$ ” mode, on the other hand, corresponds to a metallic slab that is part of an electric circuit. This mode is not as easy to implement into periodic DFT codes as the “ $N_e = \text{constant}$ ” mode. Therefore most of the calculations of metallic slabs have been performed at a constant number of electrons. There are in fact implementations of periodic DFT calculations that perform self-consistent iteration within the grand-canonical formulation of DFT [6, 20], i.e., the electron density is calculated in each iteration step as a sum of partial densities over Kohn-Sham orbitals with eigenvalues up to a given chemical potential  $\mu$  so that the number of electrons is not necessarily conserved. However, such a scheme does exhibit a rather slow convergence, much slower than calculations with a fixed number of electrons. However, also calculations in the “ $N_e = \text{constant}$ ” mode can be related to the “ $\mu = \text{constant}$ ” mode. This is done by performing calculations for different charge states, determining the corresponding potentials and interpolating the desired quantity as a function of the potential in order to get the correct value for a given arbitrary potential. This

will be demonstrated below using the oxygen dissociation [21] as an example.

## B. Energy correction in the presence of a constant charge background

Introducing a constant charge background to balance the excess charge on a metal slab is relatively easy to implement into periodic DFT codes; in fact, it corresponds to the default procedure in periodic DFT codes to compensate a charged system. However, the charged background interacts with the system under consideration. In order to compare various charged systems at constant potential that will in general be counterbalanced by different charge backgrounds, the interaction energy has to be corrected for.

The presence of the charge background leads to additional terms in the DFT energy  $E_{\text{DFT}}$  [6, 8, 9]. The derivative of the energy with respect to the charge is then given by

$$\frac{\partial E_{\text{DFT}}}{\partial q} = \frac{\partial E_{\text{sys}}}{\partial q} + \frac{\partial E_{\text{sys-bg}}}{\partial q} + \frac{\partial E_{\text{bg}}}{\partial q}, \quad (1)$$

where  $E_{\text{sys}}$  is the energy of the charged water/electrode system,  $E_{\text{sys-bg}}$  is the interaction between the system and the background charge, and  $E_{\text{bg}}$  is the energy of the background.  $E_{\text{sys-bg}}$  and  $E_{\text{bg}}$  can be expressed as

$$E_{\text{sys-bg}} = \int \rho_{\text{bg}} V_{\text{sys}} d^3x, \quad (2)$$

$$E_{\text{bg}} = \int \rho_{\text{bg}} V_{\text{bg}} d^3x. \quad (3)$$

where  $V_{\text{sys}}$  is the electrostatic potential of the charged water/electrode system and  $V_{\text{bg}}$  is the electrostatic potential of the background charge. Then the derivative (1) can be expressed as

$$\frac{\partial E_{\text{DFT}}}{\partial q} = \mu - \int \frac{V_{\text{sys}} + V_{\text{bg}}}{\Omega} d^3x \quad (4)$$

$$= \mu - \int \frac{V_{\text{tot}}}{\Omega} d^3x, \quad (5)$$

where  $\rho_e = -\rho_{\text{bg}} = q$  was used. The total energy is obtained by integrating the chemical potential  $\mu$  over the the applied charge, i.e.,

$$E = \int_0^q \mu dQ = E_{\text{DFT}} + \int_0^q \left[ \int \frac{V_{\text{tot}}}{\Omega} d^3x \right] dQ. \quad (6)$$

## C. Potential in the presence of a constant charge background

The presence of the charge background does not only affect the total energy of the considered system, it also influences the one-electron potential. Naively one could

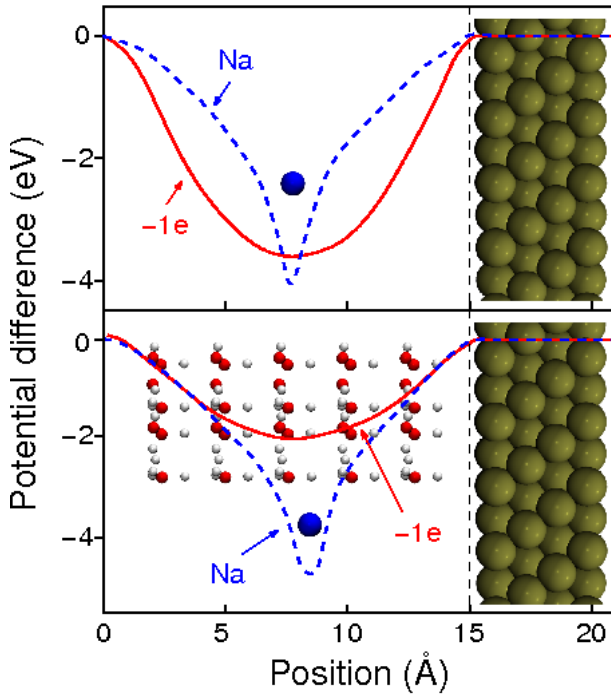


FIG. 3: Calculated potential difference between a charged and uncharged Cu(111) slabs with the excess electron density compensated either by a constant charge background (denoted by  $-1e$ ) or a sodium ion pseudopotential (denoted by Na) without (upper panel) and with a water layer (lower panel) in front of the electrode (after [9]). Note that the plotted atoms are only included as an illustration and do not correspond to the actual positions of the atoms in the calculations.

think that a constant charge background can not create any potential gradient corresponding to an electric field since it is translationally invariant. However, one has to take into account that the constant charge background is superimposed on the varying charge density of the water-metal system, and the resulting electrostatic potential as a solution of the Poisson equation is a consequence of the whole charge distribution subject to the appropriate boundary conditions. Even in vacuum regions where the charge distribution is entirely given by uniform background charge, this leads to a varying potential. This can easily be seen by inspecting the Poisson equation for a region with a constant charge background:

$$\nabla^2 \phi(\mathbf{x}) = 4\pi\rho_o. \quad (7)$$

The general solution in Cartesian coordinates is given by

$$\phi(\mathbf{x}) = 4\pi\rho_o \left( \sum_{i,j=1}^3 C_{i,j} x_i x_j + \sum_i C_i x_i + C_0 \right) \quad (8)$$

with  $\sum C_{ii} = 1$ . Note that there is no proper solution of Eq. (7) for an infinitely extended isolated uniform charge background reflecting the fact that the electrostatic energy density diverges for such a system. However, for

a finite region of constant charge density the potential follows a quadratic profile according to Eq. (8). This is confirmed in periodic DFT calculations as illustrated in Fig. 3 where in the upper panel the calculated potential difference between a charged and uncharged Cu(111) slab with the excess charge compensated by a constant charge background [9] (indicated by  $-1e$ ) is plotted. The variation of the electrostatic potential can be understood considering the fact that for positions displaced from the middle of the vacuum region there are unequal amounts of charge in the opposite directions along the surface normal.

It is obvious that this dependence of the potential in the vacuum region can create artefacts. If for example the work function of the metal is smaller than the depth of the potential minimum in the middle of the vacuum region, then there will be an unrealistic charge flow from the metal slab to the middle of the vacuum region.

Instead of balancing the excess charge of the slab by a constant charge background, one can also explicitly include counter ions at the approximate position of the outer Helmholtz plane as a model for the electrochemical interface. The corresponding potential difference is also included in Fig. 3 where the counter ion is represented by a sodium ion pseudopotential that should lead to the same formal surface charge density as in the case of the positive charge background. As Fig. 3 demonstrates, the resulting potential is quite different for the two methods. The slope of the two potential curves also differs significantly leading to an electric field that is more than a factor of two larger close to the electrode in the case of the constant charge background.

This difference is considerably reduced in an aqueous environment because of the screening effects of the polarizable water layers, as the lower panel of Fig. 3 demonstrates where the corresponding potential differences at a  $\text{H}_2\text{O}/\text{Cu}(111)$  interface are shown [9]. In particular across the inner water layer the resulting electric fields are rather similar. This suggests that the continuum technique might be appropriate to model electrochemical processes occurring in the inner layer. Still one has to be aware that the introduction of a constant charge background can introduce artefacts in the description of electrochemical interfaces.

#### D. Selection of a reference potential

In the previous section, we have shown that the explicit consideration of the aqueous environment leads to a spatial variation of the potential in the inner water layer that appears to be realistic. Still, the determination of the absolute value of the potential with respect to a well-defined reference is crucial for a true comparison with electrochemical experiments which are performed under potential control.

In the case of a neutral metallic surface, it is most convenient to define the reference potential with respect

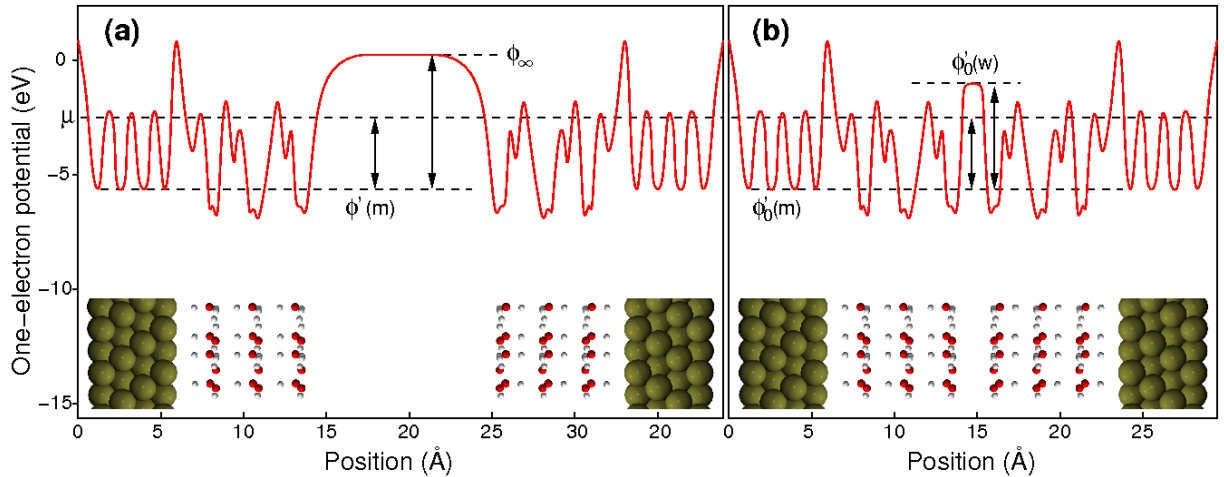


FIG. 4: Schematic illustration of the electrostatic energy profile across the unit cell in a periodic slab calculation for solvated water slabs with (a) and without (b) a vacuum layer in the middle between the metal slabs.  $\mu_e$  is the chemical potential of the electrons which corresponds to the Fermi energy at  $T = 0$  K.  $\phi_\infty$  is the vacuum level and  $\phi'(m)$  and  $\phi'_0(m)$  are bulk metal potential with and without the presence of the vacuum layer in the calculations, respectively (after [9]).

to the potential  $\phi_\infty$  far away from the surface well into the vacuum region. This potential is related to the work function  $\Phi$  and the chemical potential  $\mu$  of the electrons according to

$$\phi_\infty = \Phi + \mu \quad (9)$$

There are some subtleties about what “far away” exactly means for finite crystallites [22], but as far as periodic slab calculations are concerned,  $\phi_\infty$  is defined as the one-electron potential well in the vacuum region between the slabs where it is independent of the position within a certain spatial region.

If, however, the interstitial region between the slabs is filled with water and, in addition, the slab is charged, then it is not so obvious to define a reference potential. Taylor *et al.* have suggested a so-called “double-reference method” [9] for the situation in which the charge of the slab is compensated by a uniform background. In a first step, a DFT calculation is performed for a solvated slab with a vacuum region introduced in the middle of the unit cell between the slabs, as illustrated in Fig. 4a. For such a setup, the vacuum level  $\phi_\infty$  and the work function of the metal/water interface are computationally well-defined, as in periodic calculations for the metal/vacuum interface.

The potential in the middle of the vacuum layer is used as the first reference by setting  $\phi_\infty = 0$ . The water layer should be thick enough that the vacuum level is converged with respect to the number of included water layers in Fig. 4a. Then it is a reasonable assumption that the electrode potential does not change when the vacuum layer in the water region is omitted (Fig. 4b). A point in the interior of the metal slab is selected where the potential variation does not depend on the presence of the vacuum region. The corresponding potential  $\phi'_0(m)$

is adjusted according to

$$\phi_0(m) = \phi(m) = \phi'(m) - \phi_\infty \quad (10)$$

where the primed values indicate the unshifted values and the subscript 0 denotes the uncharged calculations without a vacuum. All other potentials in the profile are then taken with respect to  $\phi_0(m)$ :

$$\begin{aligned} \phi_0(z) &= \phi'_0(z) - \phi'_0(m) + \phi_0(m) \\ &= \phi'_0(z) - \phi'_0(m) + \phi'(m) - \phi_\infty \end{aligned} \quad (11)$$

For a charged slab, however, we are facing the problem that a variation in the electronic charge  $q$  leads to the existence of an electric field at the interface. Consequently, a vacuum reference point can not be established because there is no region where the potential is flat. Taylor *et al.* [9] suggest the following procedure to determine a reference potential: A region far from the electrode is fixed at its position in the  $q = 0$  calculation and its potential  $\phi_0(w)$  is used as the second reference point. The rest of the system is relaxed under the influence of the applied charge, and the potential at all other positions is shifted with respect to the second reference point:

$$\phi_q(z) = \phi'_q(z) - \phi'_q(w) + \phi_0(w) \quad (12)$$

Finally, the electrode potential versus the normal hydrogen electrode is obtained by subtracting the work function for the  $\text{H}_2/\text{H}^+$  couple on Pt in standard conditions,

$$\phi_{\text{NHE}} = -4.85 \text{ eV} - \phi_q. \quad (13)$$

$\phi_q = \mu$  is the Fermi potential taken with respect to the vacuum potential. For the unsolvated case it is related to the work function  $\Phi$  according to  $\phi_q = -\Phi$ , as can be derived from eq. (9) by setting  $\phi_\infty = 0$ . It has to be

subtracted here since it is defined with respect to the electrons whereas the electrode potential in electrochemistry is usually taken with respect to a positive probe charge. Note that one has to be cautious about the fact whether the potential plotted in theoretical studies is plotted with respect to a positive or a negative probe charge because it is often not explicitly specified.

In calculational setups in which an external electric field is created either by a localized planar charge distribution [23, 24] or by a dipole layer [7] in the vacuum region, the reference potential is not that easy to determine since there is no field-free space in which a vacuum level  $\phi_\infty$  could be determined. In order to define a reference electrode, the potential at the charged layer in the middle of the vacuum region can be set to zero [6, 25]. Thus results for different systems, e.g. different surface reconstructions, can be compared at the same potential. However, in this approach the position of the charged layer is an essential parameter since the calculated energies such as surface energies depend on the distance between surface and reference electrode [25].

Still, it is possible to define an experimentally meaningful potential in this approach by using the relation

$$dq = C d\phi \quad (14)$$

between the surface charge  $q$  and the electrode potential  $\phi$  which are connected via the differential capacitance  $C$  of the double layer [24]. The determination of the capacitance should in principle also be possible in the framework of DFT calculations, but it is not trivial. Thus, in a DFT study addressing the potential-induced lifting of the Au(100)-(hex) reconstruction, the surface charges were converted to electrode potential using measured values of the capacitance [24].

### III. WATER-METAL INTERFACE IN THE ABSENCE OF EXTERNAL FIELDS

The structure of the water-metal interface is naturally of strong interest in electrochemistry. However, the importance of the water-metal interaction in many aspects has also motivated numerous surface science studies (for reviews, see [26, 27]). Likewise, there is also a strong theoretical interest in the structural characterization of the water-metal interface and water-adsorbate interactions at the solid-liquid interface. We will first address, based on a recent excellent review [14], the geometric and electronic structure of water at the water-metal interface according to DFT calculations and then discuss the influence of water on molecule-surface interactions in the absence of external fields.

#### A. Structure of the water-metal interface

As far as a single water monomer on metal surfaces is concerned, it binds relatively weakly to the metal

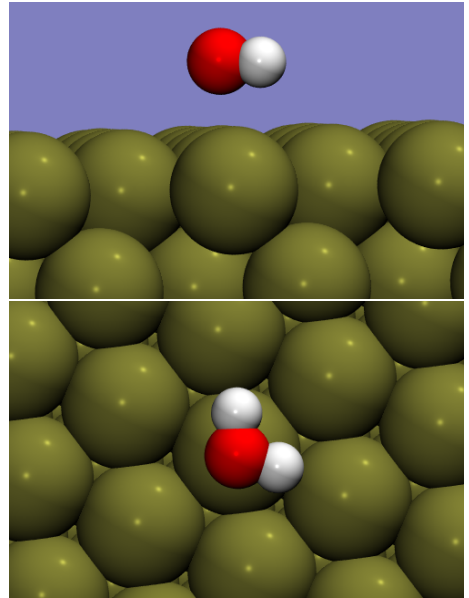


FIG. 5: Side and top view of the typical adsorption configuration of a water monomer on a close-packed metal surface.

atoms with adsorption energies ranging from -0.1 eV to -0.4 eV. As for some particular important late transition metals, the interaction strength is ordered according to  $\text{Au} < \text{Ag} < \text{Cu} < \text{Pd} < \text{Pt} < \text{Ru} < \text{Rh}$  [14]. The water monomers typically bind via their oxygen atom to the top sites of metal surfaces in an almost flat configuration, as illustrated in Fig. 5, at distances between 2.25 Å (Cu) and 3.02 Å (Au) that are much larger than typical distances of specifically adsorbed or chemisorbed species.

From the electrochemical point of view, the structure of water at a solvated metal electrode is of great interest. Still there are many uncertainties left. In particular the question whether water at the solid-liquid interface is crystalline, i.e. ice-like, or rather water-like is not fully answered yet. On late transition metal surfaces, in particular with hexagonal symmetry, it is traditionally assumed that water adsorbs in a bilayer structure [14] whose structure is similar to that of the densest layer of ice [26]. In this structure, every second water molecule is oriented parallel to the surface in a fashion similar to the water monomer shown in Fig. 5. For the other water molecules, there are in fact two different possible orientations, namely the so-called H-down and H-up structures with one hydrogen atom either pointing towards or away from the surface. These structures are illustrated in Fig. 6a and b.

The adsorption energies per water molecule on late transition metals with respect to the free water molecules range between -0.42 and -0.56 eV [14, 28]. The H-up structure is energetically favorable on Ni(111), Cu(111) and Ru(0001), whereas on Rh(111), Ag(111), Pt(111), Pd(111) [14] and Pd/Au(111) [7] the H-down structure is more stable. In this context it should be mentioned that these energies are less negative than the calculated subli-

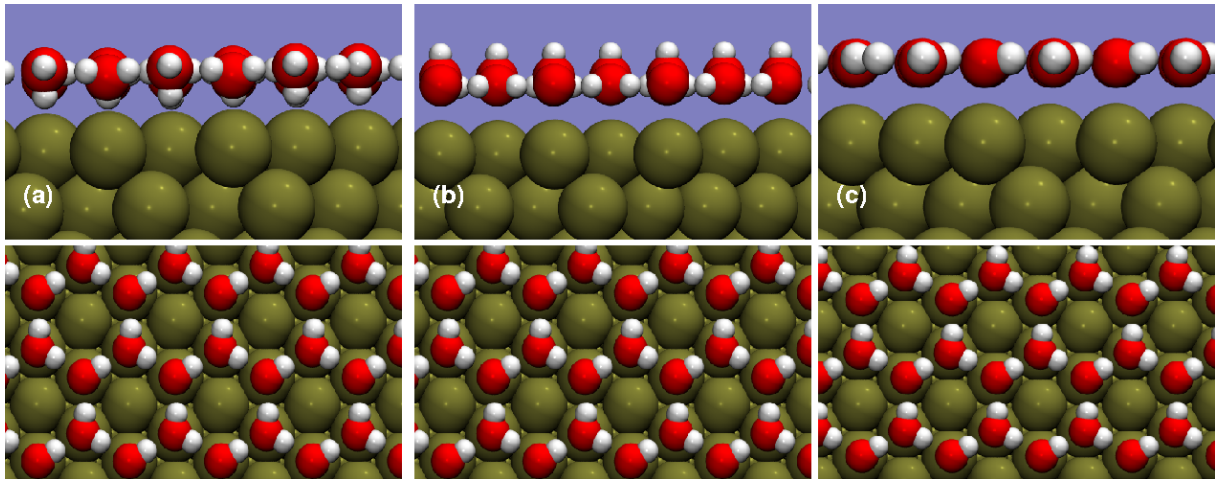


FIG. 6: Side and top view of the water bilayer structures: a) H-down bilayer, b) H-up water bilayer, c) half dissociated water-OH-bilayer with the additional hydrogen atoms being removed.

mation energy of water in a 32-molecule per cell model of ice-Ih,  $E_{sub} = -0.666$  eV [7]. This means that the considered water adlayers are not thermodynamically stable with respect to conversion to a three-dimensional ice cluster. This might be an indication that the metal-water interaction is underestimated by current DFT functionals.

Therefore it is of interest to decompose the computed adsorption energies in the bilayer structures into the contribution from the water-metal and the water-water interaction. Unfortunately it turns out that there is no unique decomposition of the water adsorption energies into these two contributions [7, 14]. One can assume that the bilayer is first assembled in the gas phase and then deposited on the electrode surface. Alternatively, one can first adsorb the water molecules individually on the surface and then assemble the ice-like bilayer structure. The first approach does not take into account the changes of the inter-water binding during the adsorption of the water bilayer whereas the second approach assumes that the water-metal interaction stays constant when the water bilayer is assembled.

However, although there are small quantitative differences in the two energy decomposition schemes outlined above [7, 14], qualitatively they yield rather similar results. The main result is that most of the binding energy in the water bilayers (about 75%) comes from the water-water interaction whereas the water-metal interaction is rather weak with binding energies below 0.2 eV per water molecule. Interestingly enough, the water-water interaction on the considered close-packed surfaces is found to be almost independent of the lattice spacing [14], although the next nearest neighbor lattice distance between equivalent water molecules spans values from 4.33 Å for Ni to 5.04 Å for Ag whereas the corresponding calculated equilibrium value for ice  $I_h$  is 4.50 Å. This is in fact surprising since one would expect that the hydrogen-bonding between the water molecules exhibits a stronger depen-

dence on the distance.

The water bilayers might in fact not stay intact on the electrode surfaces. Feibelman had suggested on the basis of DFT calculations that water on Ru(0001) should form a half-dissociated overlayer [29] where every second water molecule is dissociated to OH. Such a  $H_2O-OH$  structure with the additional hydrogen atoms being removed is illustrated in Fig. 6c. As a matter of fact, Ru is not the only metal where half-dissociated water layers are more stable. In Fig. 7, the bilayer dissociation energy is plotted which corresponds to the total energy difference between the most stable intact bilayer and the half-dissociated water overlayer per unit cell where the extra hydrogen atom is assumed to be adsorbed at its most favorable threefold hollow site on clean portions of the metal. The negative values for Ru, Rh and Ni indicate that the half-dissociated water overlayer is more stable whereas on Cu, Pt and Ag the water bilayers rather stay intact, and Pd is an undecided case. The dissociation energies in Fig. 7 are plotted against the OH adsorption energies at the ontop sites of the respective surfaces showing a clear correlation. The less noble metals Ru, Rh and Ni bind OH more strongly than the more noble metals which apparently provides a driving force for the water dissociation. Still it is not clear whether the water layers indeed dissociate since the formation of the partially dissociated overlayers might be kinetically hindered by the presence of high barriers.

In order to assess the influence of the presence of water on the interaction of molecules with electrode surfaces it is interesting to inspect the changes of the electronic structure at the surface upon the adsorption of water. In Fig. 8, the local density of states (LDOS) of the clean Pt(111) surface is compared with those of water-covered surfaces [30]. For the H-down water bilayer shown in Fig. 6a, there are three inequivalent Pt surface atoms per surface unit cell, either non-covered or covered by a water molecule bound via an oxygen atom or a hydrogen

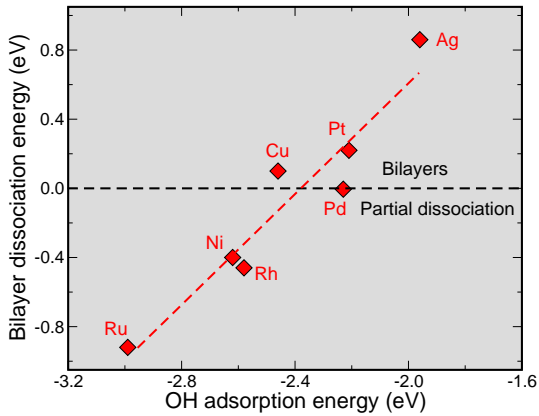


FIG. 7: Bilayer dissociation energy as a function of the OH adsorption energy at atop sites (after [14]).

atom. The LDOS of these Pt atoms is similar to the one of bare Pt(111). This indicates that there is a rather weak interaction between water in the bilayer structure and metal electrode surfaces with binding energies below 0.2 eV, as discussed above.

An isolated water monomer, on the other hand, is bound by 0.35 eV to Pt(111) [30]. This stronger interaction leads to a more pronounced modification of the LDOS of the Pt atom closest to the water monomer. In particular the peak at about -4.5 eV is caused by the hybridization of the water  $1b_1$  orbital with the Pt  $d$ -band [31]. Still it should be noted that also in the case of water monomer adsorption the water-induced change in the electronic structure of Pt is small, some peak heights of the LDOS are altered but the peak positions and their width remain almost the same.

Although the adsorption energy of the H-up and H-down water bilayers are usually rather similar, there is a strong dependence of the bilayer-induced work function change  $\Delta\Phi$  of the metal electrodes on the orientation of the water bilayer resulting in differences in  $\Delta\Phi$  of about 2.2 eV on Pd(111) [32] and 2.0 eV on Pt(111) for the two orientations. It has already been noted that this large difference leads to a charge control of the water monolayer/metal interface, i.e., the stable water bilayer structure can be tuned by changing the surface charge [32]. It is not surprising that the effect of the H-up and H-down water bilayers on the work function is so different because their associated dipole moments have different signs. However, it is quite surprising that on Pd(111) [32] as well as on Pt(111) both types of bilayers lower the work function. The H-down water bilayer induced work function change is  $\Delta\Phi = -0.23$  eV, whereas it is  $\Delta\Phi = -2.27$  eV for the H-up water bilayer. Naively one would expect that because of the oppositely oriented dipole moments the H-down bilayer would lower the work function while the H-up bilayer would increase the work function.

In order to understand this astonishing result, it is

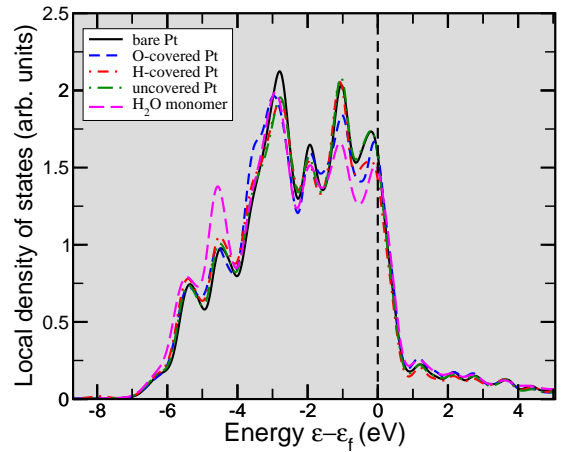


FIG. 8: Local density of states (LDOS) of the Pt(111) surface atoms without and in the presence of water. For the H-down water bilayer the LDOS of the three inequivalent Pt atoms within the surface unit cell is shown whereas for the adsorption of the water monomer only the LDOS of the Pt atom directly below the water molecule is plotted (after [30]).

instructive to analyze the charge density difference

$$\Delta\rho = \rho(\text{H}_2\text{O}/\text{Pt}(111)) - (\rho(\text{H}_2\text{O}) + \rho(\text{Pt}(111))) , \quad (15)$$

which corresponds to the water adsorption-induced rearrangement of the charge density. In Fig. 9, the laterally averaged charge density difference as a function of the position perpendicular to the surface for both types of bilayers is plotted. Since oxygen is more electronegative than hydrogen, the free H-up bilayer has a dipole moment that lowers the work function. In addition, due to the interaction of the water layer with the Pt(111) surface electronic charge flows from the water layer to a region close to the Pt atoms. Figure 9 also shows the integral of the density difference along the surface normal, and the position of its maximum roughly separates the regions of charge surplus and charge deficiency. This charge rearrangement causes an additional effective dipole layer that further lowers the work function.

In the case of the H-down water bilayer on Pt(111), there is even a much stronger charge flow from the water layer to the region between metal and water layer. The water layer itself has a dipole moment that would increase the work function of the surface, but the charge rearrangement is so large that the resulting effective dipole moment overcompensates the dipole moment of the water layer leading to a net reduction of the Pt(111) work function by 0.23 eV.

Figure 9 also indicates that there is some charge rearrangement within the Pt(111) slab upon the interaction with water, but is rather small, which is consistent with the minor changes observed in the Pt(111) local density of states in Fig. 8. Thus the overall lowering of the Pt(111) work function in the presence of both the H-up as well as the H-down water bilayers is mainly a consequence of the high polarizability of water.

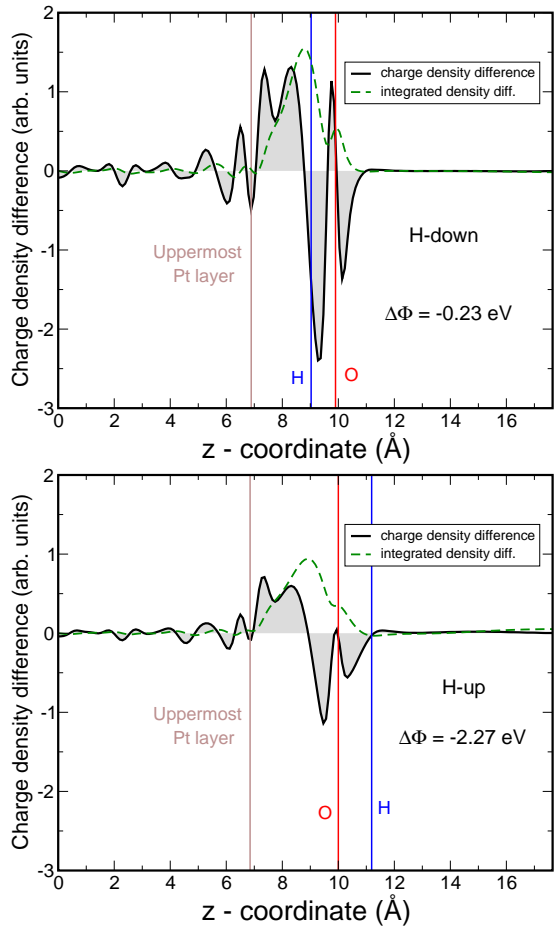


FIG. 9: Laterally averaged charge density difference and its vertical integrated value upon the adsorption of a H-down and a H-up water bilayer, respectively, on Pt(111) as a function of the position perpendicular to the substrate. The vertical lines indicate the position of the uppermost Pt atoms, the oxygen atom and the H-down and H-up atom, respectively.

The geometric and electronic structure discussed so far are related to static properties of adsorbed water in equilibrium geometries. However, processes in electrochemistry occur at temperatures close to room temperature so that the observed experimental properties correspond to thermal averages. Furthermore, the dynamics of the water layer itself is interesting for an understanding of electrochemical processes on metal surfaces. The structure of the Ag(111)-water interface was addressed by ab initio molecular dynamics (AIMD) simulations [33] based on the Car-Parrinello scheme [34]. In this study, the initial configuration for the AIMD runs was obtained from a classical MD simulation, employing a model chemisorption metal-water potential [12], that was performed for a system of 256 water molecules for 30 ps at a temperature of about 300 K in a  $c(8 \times 4)$  surface unit cell. The positions of the 48 water molecules closest to the surface were then used for the initial configuration of the AIMD simulation that was run for 2.1 ps.

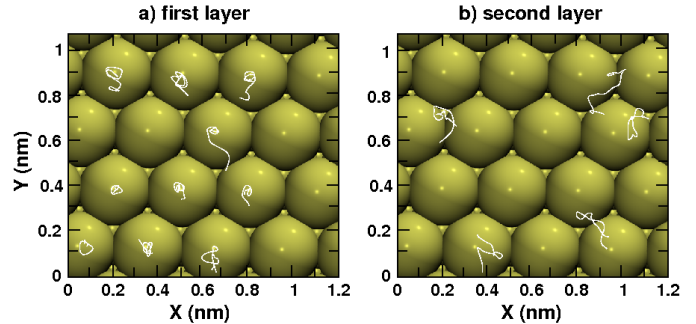


FIG. 10: Trajectories of ab initio molecular dynamics runs of water on Ag(111) of the water molecules in the first layer (a) and of selected molecules of the second layer (b) (after [33]).

AIMD trajectories of the water molecules in the first layer within the surface unit cell are shown in Fig. 10a. In these simulations, all water molecules were bound via the oxygen atom to the top sites of the Ag(111) surface. As the trajectories indicate, the water molecules in the first layer remain rather localized above the top sites. The molecules of the second layer seem to be more mobile, as the plotted trajectories of selected molecules in Fig. 10b suggest. Interestingly enough, the configuration of the water molecules in the first layer (Fig. 10a) does not exhibit any indication of a hexagonal bilayer structure although the coverage of 0.63 is roughly the same as in the bilayers. It is not clear whether this is an artefact of the parameterized potential used to determine the initial configuration or whether this is a consequence of the non-zero temperatures.

In order to derive experimentally whether the water structure at the water-electrode interface is crystalline or rather disordered, measured vibrational spectra have been analyzed [35], in particular focusing on the OH stretch vibration in the range between 2800 and 3800  $\text{cm}^{-1}$ . Generally, OH stretch vibrations at about 3200  $\text{cm}^{-1}$  have been assigned to three-fold coordinated water, i.e., water in a disordered liquid-like structure, whereas OH stretch vibrations at about 3400  $\text{cm}^{-1}$  have been taken as a signature of four-fold coordinated water, i.e., highly-ordered ice-like water molecules [36]. While for Pt(111) two broad peaks at 3200  $\text{cm}^{-1}$  and 3400  $\text{cm}^{-1}$  were obtained [35], the observed vibrational spectra on Au(111) were dominated by a broad peak around 3500  $\text{cm}^{-1}$ ; however, this peak was attributed to oxide formation. The results were interpreted as being an indication that on Pt(111) ordered and disordered water structures coexist whereas on Au(111) the water is less well-ordered.

Vibrational spectra can be evaluated from molecular dynamics runs performing a Fourier transformation of the velocity auto-correlation function [37]. We have performed AIMD simulations of H-down water bilayers on Pt(111) and Ag(111) for 5 ps with a time step of 1 fs within a  $2\sqrt{3} \times 2\sqrt{3}$  surface geometry at a temperature of 300 K based on periodic DFT calculations [15] using

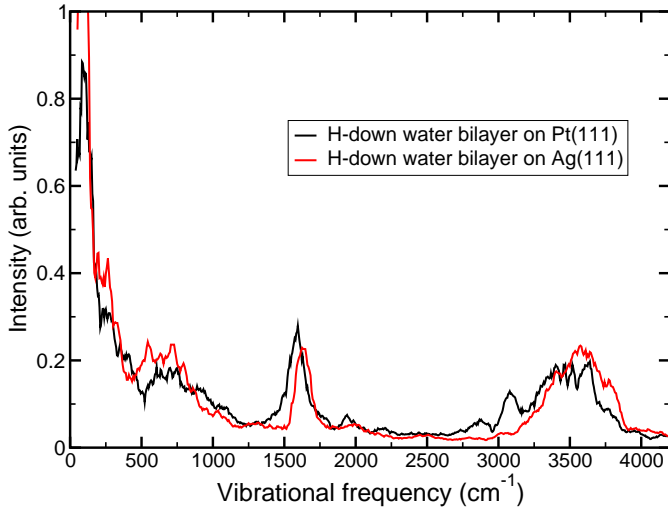


FIG. 11: Calculated vibrational spectrum of H-down water bilayers on Pt(111) and Ag(111) derived from *ab initio* molecular dynamics (AIMD) simulations that have been run for 5 ps in a  $2\sqrt{3} \times 2\sqrt{3}$  geometry at a temperature of 300 K.

the PBE functional [16]. These conditions lead to a spectral resolution of  $\delta\omega \sim 6\text{cm}^{-1}$  [37]. The resulting spectra are plotted in Fig. 11. Two main peaks are obvious, around  $3500\text{cm}^{-1}$  and around  $1600\text{cm}^{-1}$  which are related to the OH stretch and bending vibrations, respectively. First of all it is obvious that the water vibrations on Pt(111) are red-shifted compared to those on Ag(111) which can be explained by the stronger Pt-water interaction compared to the Ag-water interaction. Interestingly enough the spectra are rather similar to the experimentally measured spectra on Pt(111) and Au(111) [35], in particular as far as the existence of two peaks on Pt(111) is concerned, although no disordered structures evolved on Pt(111) in the AIMD simulations. On Ag(111), on the other hand, the simulations indeed suggest that the water layer might become disordered at room temperature.

### B. Influence of water on the molecule-metal interaction

The field of electrocatalysis is concerned with reactions of molecules at electrode surfaces in an electrochemical environment. In this context, it is of course interesting how the presence of water influence molecule-metal interactions. In the previous section we have shown that adsorbed water bilayers become strongly polarized but that their presence only weakly influences the electronic structure of the substrate. Thus it is not clear how much the presence of water bilayers modifies adsorption energies in specific adsorption.

This issue was addressed in a DFT study of CO and hydrogen adsorption on a bimetallic PdAu surface consisting of a pseudomorphic Pd overlayer on Au(111) [7].

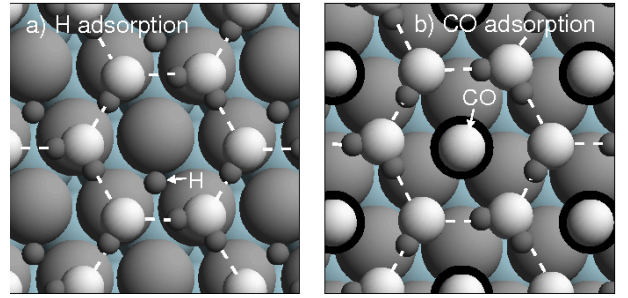


FIG. 12: Relaxed adsorption geometry of the H-down bilayer on the Pd/Au(111) overlayer system together with adsorbed hydrogen (a) and CO (b)(after [7]).

In Table I, the hydrogen and CO adsorption energies on the clean substrate and in the presence of H-down and H-up water bilayers are collected. In the presence of water bilayers, the binding of hydrogen and CO to Pd/Au(111) becomes weaker, but only by less than 10%. For hydrogen, the results are basically independent of the specific form of the water bilayer. For CO, the change in the binding due to the presence of water is somewhat larger than for hydrogen, and also the results for the two orientations of the water bilayer differ by about 60 meV.

In order to understand these trends one should note that the height of the hydrogen atom above the plane of the Pd atoms is only  $0.6\text{\AA}$  whereas the carbon atom of the adsorbed CO is located about  $1.2\text{\AA}$  above the Pd atoms [38]. The water molecules, on the other hand, are more than  $2\text{\AA}$  above the metal atoms, as for example Fig. 9 indicates. Thus the hydrogen adsorption energies are only weakly influenced by the presence of water because the H atoms are located so close to the surface and water has only a minor effect on the electronic structure of the metal substrate. The CO molecules are located further away from the surface. Hence they will directly interact with the polarized charge distribution of the water bilayer which leads to a larger modification of the adsorption energies; furthermore, there is also a dipole-dipole interaction between the adsorbed CO molecules and the water layer that causes the dependence of the CO adsorption energy on the orientation of the water bilayer.

The water bilayers are not only weakly interacting with metal electrodes, their adsorption energy does also not strongly depend on the adsorption site. As Fig. 6 indi-

TABLE I: Hydrogen and CO adsorption energies in eV at the most favorable adsorption site on the Pd/Au(111) overlayer system on the clean surface and in the presence of H-down and H-up water bilayers [7]. The H adsorption energies is taken with respect to the free  $\text{H}_2$  molecule.

	Adsorption energies on Pd/Au(111) (eV)		
	clean	H-down bilayer	H-up bilayer
H (fcc)	-0.690	-0.661	-0.660
CO (hcp)	-2.043	-1.866	-1.923

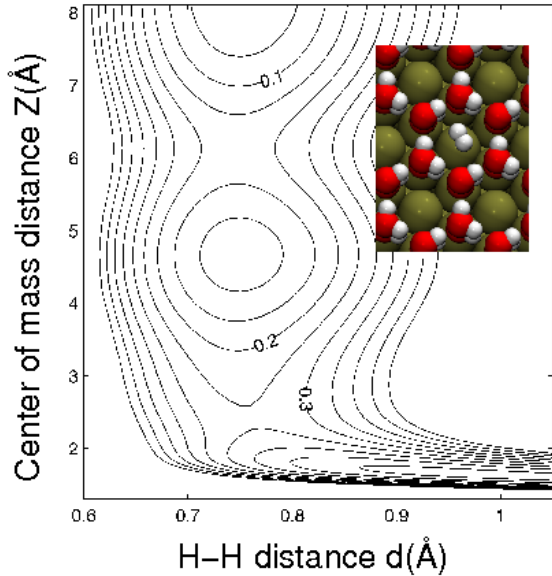


FIG. 13: Two-dimensional cut through the potential energy surface of the interaction of  $H_2$  with Pt(111) covered by two water bilayers. The potential energy is plotted as a function of the H–H distance  $d$  and the  $H_2$  center of mass distance  $Z$  from the surface. The lateral position and orientation of the  $H_2$  molecule correspond to a fcc hollow-top-hcp hollow configuration, as indicated in the inset. The contour spacing is 50 meV (after [30]).

cates, in their equilibrium structure the hexagonal rings of the water bilayers are arranged around a metal atom that remains uncovered. Now for both hydrogen and CO the most favorable adsorption site on Pd/Au(111) is the three-fold hollow site (see Table I). The fact that the hydrogen and CO binding energies on Pd/Au(111) are reduced in the presence of water demonstrates that there is a repulsive interaction between these adsorbates and water. Since the adsorbed hydrogen atom and the water bilayer are only weakly interacting, the water bilayer is only slightly distorted due to the presence of the hydrogen atoms, as Fig. 12a indicates where a top view of the energy minimum structure is shown. CO and water are interacting more strongly. Furthermore, CO is bound more strongly than the water molecules. As a consequence, the presence of adsorbed CO in three-fold hollow positions causes a shift of the water bilayer to maximize the water-CO distance.

These results show that binding energies in specific adsorption are weakly influenced by solvation effects, as long as the adsorbates are located close to the electrodes. However, transition state configurations of electrocatalytic reactions are often further away from the surface than the adsorption sites which might lead to a larger effect of water on the reaction. As a simple example, the influence of water layers on the dissociation of  $H_2$  above Pt(111) was studied [30].

A two-dimensional cut through the potential energy

surface of  $H_2$ /Pt(111) in the presence of a water double layer is plotted in Fig. 13 as a function of the H–H distance  $d$  and the  $H_2$  center of mass distance  $Z$  from the surface [30]. Note that on the clean Pt(111) surface  $H_2$  dissociation is only hindered by a barrier of 54 meV. At the solvated surface, this barrier is increased by 167 meV to a value of 221 meV. This barrier is located roughly at the position of the first water bilayer above the surface. It is interesting to note that the increase in the barrier height approximately corresponds to the barrier for  $H_2$  to propagate through a free water bilayer which is very similar to the barrier for the  $H_2$  propagation through the upper water bilayer at a height of about 6 Å above the surface, as shown in Fig. 13. Thus to a first approximation the barrier for the  $H_2$  dissociative adsorption at a Pt(111) surface solvated with ice-like water can be regarded as a superposition of the dissociation barrier for the bare surface plus the barrier for propagation through the water bilayer which indicates that the modification of the barrier is not the result of any water-induced modification of the electronic structure of Pt(111).

#### IV. WATER-METAL INTERFACE IN THE PRESENCE OF EXTERNAL FIELDS AND/OR VARYING ELECTRODE POTENTIALS

So far we have only considered the structure of water bilayers on metal surfaces and their interaction with molecules without any external field. These calculations are certainly relevant for the understanding of basic processes in electrocatalysis. Furthermore, even if no external field is considered, the setup corresponds to a certain electrode potential that could in principle be determined. However, in electrocatalysis the basic quantity of interest is the given electrode potential. Here we will describe approaches to describe external fields and/or varying electrode potentials in the framework of periodic DFT calculations.

##### A. Modeling electric fields through a dipole layer

In periodic slab calculations, it is a standard procedure to correct the dipole moment of a non-symmetric slab along the surface normal by a planar dipole layer in the middle of the vacuum region in order to electrostatically decouple the periodically repeated slabs [18]. Yet, the dipole layer can also be used to create an external electric field acting on the slab. This approach was employed in a DFT study to address the stability of the H-down and H-up water bilayers on the Pd/Au(111) pseudomorphic overlayer system as a function of an external electric field [7]. Because of the oppositely oriented dipole moments of the H-down and H-up water bilayers, they should react differently to an applied external electric field.

Figure 14 shows the calculated effective one-particle

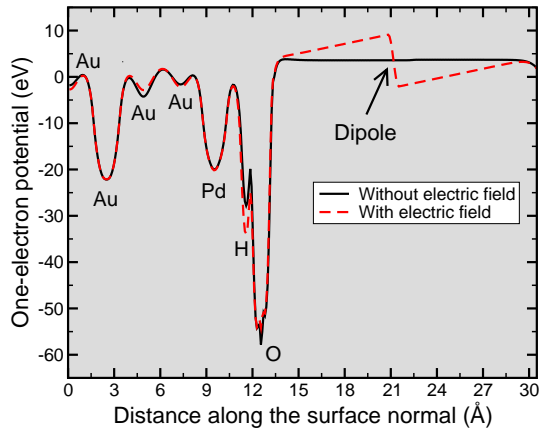


FIG. 14: Effective potential along the surface normal  $z$  which passes through the water layer for zero external field and with an electric field of strength  $E = -0.7 \text{ V/\AA}$  (after [7]).

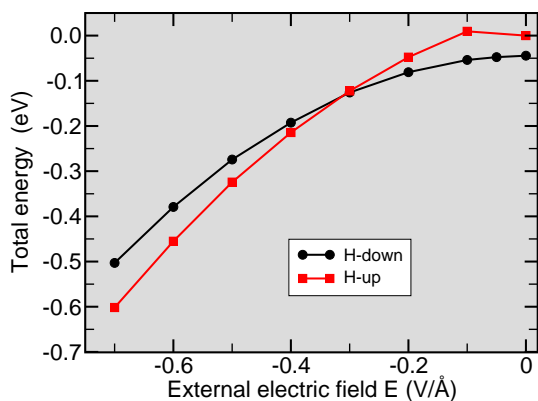


FIG. 15: Change of the total energy of the H-down and H-up water bilayers as a function of an external electric field. The energy zero corresponds to the H-up structure without any external electric field (after [7]).

potential through a water layer on a Pd/Au(111) bimetallic overlayer system without and with an external electric field which is created by a dipole layer whose position is indicated. The slope of the potential in the vacuum region corresponds to the applied electric field. Note that inside the metal electrode, the one-particle potential is hardly affected demonstrating the good screening properties of metals. In the water layer, the potential is slightly modified by the presence of the electric field.

Surface X-ray scattering experiments had found a surprisingly large inward contraction of the water molecules for positive electrode potential [39, 40]. However, electric fields with a strength of up to  $0.5 \text{ V/\AA}$  only lead to displacements of the atoms in the water bilayer by less than  $0.05 \text{ \AA}$ . Still, the applied electric field has a significant affect on the stability of the water layers, as Fig. 15 demonstrates. There the total energy of the H-down and H-up water bilayer as a function of the external electric field is plotted. Whereas in the field-free case the H-down structure is more stable, for external elec-

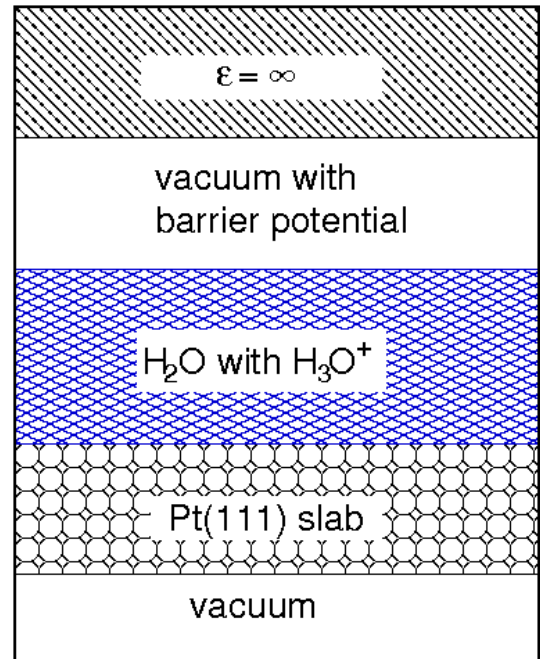


FIG. 16: Computational setup used by Sugino *et al.* [42, 43] to model the water/Pt(111) interface under bias potential within the effective screening method.

tric fields more negative than  $-0.3 \text{ V/\AA}$  the H-up bilayer becomes energetically favorable. This is in qualitative agreement with experiments for water on Ag(111) which found a field-induced rotation or flip of adsorbed water molecules [40, 41].

## B. Explicit consideration of a counter electrode

Instead of including a dipole layer a counter electrode may be explicitly considered. Some authors have used a localized planar charge distribution with a Gaussian shape perpendicular to the surface [23–25] in order to address the reconstruction of charged surfaces. In this approach, the excess surface charge is easy to determine since it corresponds to the charge of the counter electrode. These computational studies did not consider any explicit water layers at the metal surface. As already discussed in section IID, in this setup it is not straightforward to obtain the corresponding electrode potential; it was done by either using relation (14) with experimentally derived capacities [24] or by setting the potential at the position of the charged layer to zero [25]. As a general results these calculations showed that to first order in the surface charge, additional positive charges favor surfaces with smaller work function whereas negative charges favor surfaces with larger work function [25].

The so-called “effective screening method” (ESM) was suggested by Sugino *et al.* [42, 44] based on a scheme for the electronic structure calculations that is periodic in lateral direction but not in the direction perpendicu-

lar to the surface. In this method which is schematically illustrated in Fig. 16 the laterally periodic slab covered by water and/or adsorbates is placed between two polarizable continua characterized by their dielectric constant  $\epsilon$ . In order to model an electrochemical cell, the simplest model is to use vacuum ( $\epsilon = 1$ ) at the metal side and a perfect conductor ( $\epsilon = \infty$ ) at the other side. The corresponding electrostatic potential across the system is obtained from the Laplace equation using a Green's function solver [44]. The water layer was modeled by 32 water molecules within a  $(3 \times 2\sqrt{3})$  unit cell leading to four bilayers. To have acidic conditions, one proton was added to the water layer. The structure of this system was then studied by *ab initio* molecular dynamics simulations. To prevent the water bilayers from desorbing and the electrons from entering the perfect conductor, additional barrier potentials were introduced.

The bias can be varied in this approach by adding excess electrons to the system. These excess charges will induce opposite surface charges in the perfect conductor. The perfect conductor is placed approximately 20 Å above the uppermost Pt layer; hence the counter charge is located relatively far away from the Pt electrode. Since this setup does not have a three-dimensional periodicity, there is no need for compensating charges. The introduction of the excess electrons leads to the creation of a uniform electric field. During the initial thermalization of the system in the MD run which takes several ps, the double layer is formed and the potential profile becomes almost flat perpendicular to the layer due to the strong polarization of water [43]. Thus a corresponding electrode potential can be derived.

The AIMD production runs have been performed for 4 ps with excess charges of 0, 0.35, and 0.70  $e$  per supercell corresponding to potentials of 0.04, 0.36, and 0.81 V, respectively, with respect to the potential of zero charge [43]. It is found that the density of the first water layer at the electrode, the so-called contact layer, is only slightly increased by raising the potential. The rearrangement within the layers, however, becomes strongly modified for higher potentials leading to a smaller binding between the contact layer and the bulk water above the first layer. It has been speculated whether this an indication for a hydrophobic water monolayer, as suggested on the basis of experiments [45].

### C. Uniform compensating charge background

Using a uniform charge background to compensate the surface excess charges has been used in a number of studies addressing electrochemical systems at the solid/water interface [8, 9, 21, 32]. Here we will use a study of the dissociation of oxygen on Pt(111) in the presence of water and co-adsorbates as a function of the electrode potential [21] as an illustration of this method.

In this work, the  $O_2$  dissociation was studied on Pt(111) within a  $3 \times 3$  surface unit cell on the clean

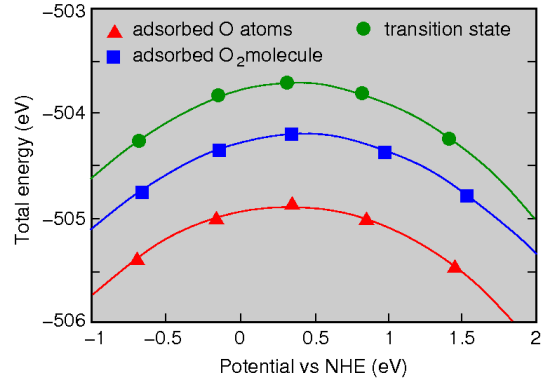


FIG. 17: Total energies versus potential for the initial, transition and final state of  $O_2$  dissociation on solvated Pt(111). The solids curves are quadratic fits to the results (after [21]).

surface, and on Pt(111) covered with one Na atom per surface unit cell. Water was included in the simulation either as a single molecule or as four ice-like bilayers. The non-solvated slab was kept symmetric, i.e., the adsorbates were added to both sides of the slab for a direct evaluation of the work function and in order to avoid spurious dipole-dipole interactions in the case of Na adsorption because of the strongly ionic Na-Pt bond.

The water structure was obtained by adding 24 water molecules to the  $3 \times 3$  surface unit cell in an ice-like structure leading to four bilayers. For the solvated slab, adsorbates were introduced into the system by replacing water molecules with them. For  $O_2$ , 2O or Na adsorption, a single  $H_2O$  molecule, while for the coadsorption of Na with  $O_2$  or 2O two  $H_2O$  molecules were replaced, and then the resulting structures were optimized. In addition, the transition state between the configurations for the  $O_2$  and the 2O adsorption was located using automatic transition state search routines [46, 47]. All these calculations were performed for different charge states of the Pt electrode by adding charges corresponding to  $-1, -0.5, 0, 0.5$  and  $1e$  to the system which were compensated by an uniform charge background. For the initial and the final states of the  $O_2$  dissociation as well as for the transition state, the potential was derived using the double-reference method [9] described in section II D, as a variation of the geometric configuration along the reaction path can also lead to a change in the work function.

Hence these calculations have not been performed for a given specified value of the potential, but rather for a given charge state, and the corresponding potential has been derived *a posteriori*. In order to yield the energies of the considered states for any arbitrary value of the potential, the results for the different charge states can be interpolated as a function of the electrode potential generating a continuous energy versus potential curve for each state. This is illustrated in Fig. 17, where the potential dependence of the initial, transition and final state energies for the  $O_2$  dissociation on the solvated Pt(111) slab is plotted. The symbols denote the total energies for

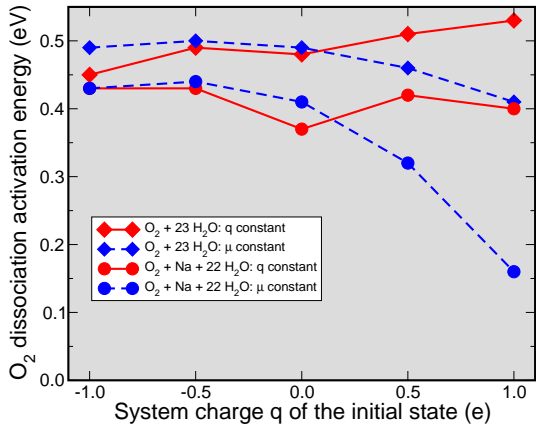


FIG. 18: Dissociation barrier of  $O_2$  on solvated Pt(111) without and with Na coadsorption denoted by  $O_2 + 23 H_2O$  and by  $O_2 + Na + 22 H_2O$ , respectively, for various system charges  $q$  of the system and for constant potential. In the latter mode, the potential of the initial state has been used as the reference and been kept fixed (after [21]).

the different states at the five different charge states considered whereas the solid curves correspond to quadratic fits to the results.

There is in fact a rationale for using a quadratic fit, as it can be regarded as an expansion of the energy as a function of the potential about the potential of zero charge ( $\phi_{pzc}$ ):

$$E(\phi) = \frac{1}{2}C(\phi - \phi_{pzc}) + E_{pzc}, \quad (16)$$

where  $C$  is the capacitance, and  $E_{pzc}$  is the energy of the system at zero charge. The fact that the curvature of the three curves is not identical indicates that the capacitance of the system depends on the actual atomic configuration.

A similar fit as shown in Fig. 17 was also made for the  $O_2$  dissociation barrier on the solvated slab with an additional Na atom. From a figure as Fig. 17, the  $O_2$  dissociation barriers can be read off for constant charge and for constant potential. The energy difference between the symbols correspond to the dissociation barrier at constant charge, whereas the energy difference of the curves for any given value of the potential corresponds to dissociation barrier at constant potential. Thus, if the symbols for a particular value of the charge are aligned vertically above each other, then the dissociation barrier are the same in the constant charge and in the constant potential mode. However, an inspection of Fig. 17 reveals that this is in general not the case.

The  $O_2$  dissociation barriers on solvated Pt(111) without and with Na coadsorption for various system charges are plotted in Fig. 18 and compared to the values for constant charge where the potential of the initial state has been kept constant. It is obvious that for negative excess charges, there is only a small difference between the constant charge and the constant potential mode, whereas

for positive charges corresponding to positive potentials there is a significance difference. The Na coadsorption has two effects. First, it reduces the  $O_2$  dissociation barrier at all given charge states and potentials. And second, it makes the potential dependence of the  $O_2$  dissociation barrier much more dramatic. These effects have been attributed to the enhanced polarizability of the system when Na is coadsorbed, however, the exact mechanism is not easy to resolve because of the complexity of the system [21]. Most importantly, the differences between the results in the constant charge and the constant potential mode indicate that it is crucial to consider the electrode potential for the determination of reaction energies in electrochemical systems.

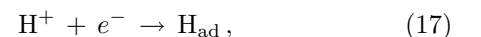
#### D. Explicite consideration of counter ions

We have already seen in the example of the work by Sugino *et al.* presented in section IV B that counter ions such as protons can of course be added to the water layer. This approach can be taken further by varying the number of electrons/protons in the double layer and thus changing the electrode potential. This can be achieved by introducing coadsorbates such as hydrogen to the system [10, 48]. The added hydrogen atoms become solvated as protons leading to the formation of hydronium ions ( $H_3O^+$ ), and the electrons move to the metal electrode. By changing the hydrogen concentration, the surface charge and hence the electrochemical potential can then be varied. In this setup, the whole supercell always remains neutral so that no countercharges are needed.

This approach has been used to address the hydrogen evolution reaction in an electrochemical double layer on Pt(111) [10]. In this study, one adsorbed water bilayer on Pt(111) was considered. The potential was varied by adding one to four hydrogen atoms to a  $(6 \times 4)$  supercell, one and two hydrogen atoms to  $(6 \times 2)$  or  $(3 \times 4)$  supercells, and one hydrogen atom to a  $(3 \times 4)$  supercell.

The variation of the electrode potential as a function of the adsorbed hydrogen atoms is illustrated in Fig. 19 where the one-electron potential is shown for two different concentrations of hydrogen atoms, one or four atoms per  $(6 \times 4)$  supercell. The underlying inset illustrates the atomic configuration. The corresponding electrode potential can be derived from the work function of the system given by the flat potential in the vacuum region. Note that the potential is averaged in lateral direction, therefore the potential variations are quite different from, e.g., those shown in Fig. 14 where the potential along one particular line is shown.

This setup has been used to study the elementary processes occurring in the hydrogen evolution reaction on Pt(111), namely the Volmer reaction



the Tafel reaction



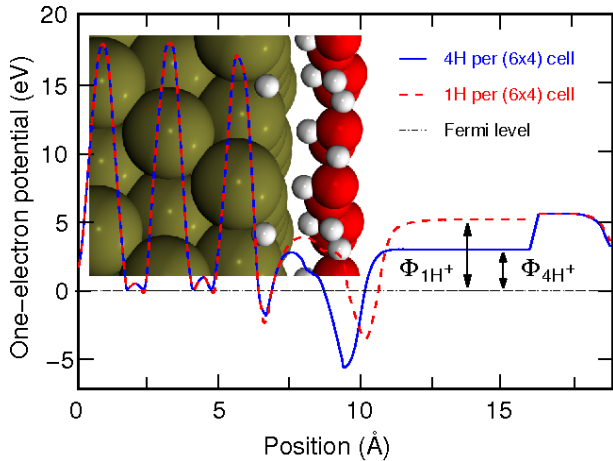
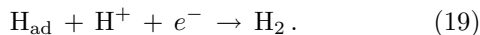


FIG. 19: One-electron potential averaged in lateral direction as a function of the position along the surface normal for two different hydrogen coverages and hence two different electrode potentials. In the vacuum layer, there is a potential drop due to the presence of a dipole layer (after [10]). The inset illustrates the structure of the interface with additional protons.

and the Heyrovsky reaction



Here we will concentrate on the Tafel reaction since it is the reverse reaction of the dissociative adsorption of  $\text{H}_2$  on Pt(111) discussed in section III B. In order to calculate the barrier of the Tafel reaction as a function of the electrode potential, first the equilibrium hydrogen coverage as a function of the potential was determined which can be derived from the differential adsorption energies as a function of the coverage [10]. Then the barrier for the Tafel reaction was evaluated for different hydrogen coverages and related to the corresponding potentials. This relationship is plotted in Fig. 20 at the electrode-vacuum interface and in the presence of a water bilayer. The same is plotted also for the Heyrovsky reaction (19). Note that the calculated data points for the Heyrovsky reaction at more negative and more positive potential are not shown.

There is a large gap between the results at negative and at positive potentials. This is caused by the fact that there is a discontinuity in the differential hydrogen adsorption energies once the coverage becomes larger than 1. The gap in Fig. 20 could only be closed if larger unit cells were chosen. Furthermore, according to Fig. 20, the barrier for the Tafel reaction is not changed significantly by the presence of the water [10]. This seems to be at variance with the results by Gohda *et al.* [30] discussed in section III B who found that the presence of water leads to an increase of the barrier for the inverse Tafel reaction by about 170 meV. This seemingly inconsistency of the results is resolved when one considers that the presence of water also leads to a reduction of the atomic hydrogen binding energies from 468 meV at the clean Pt(111)

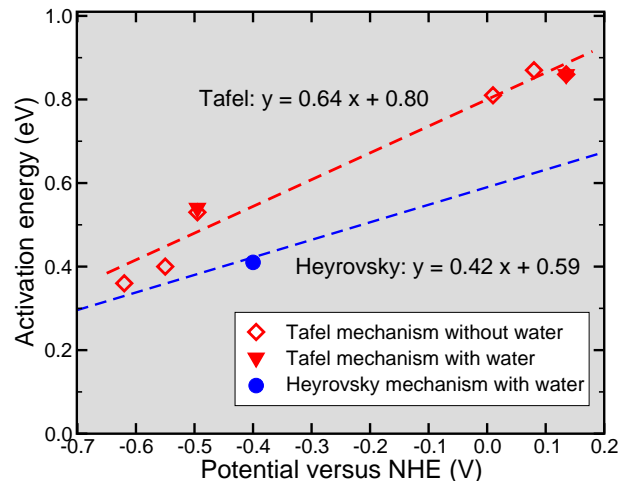


FIG. 20: Calculated activation energy for the Tafel reaction as a function of potential without (diamonds) and with (triangles) a water bilayer and for the Heyrovsky reaction with water (circles) (after [10]). For the Heyrovsky reaction, two further barriers were determined which lie outside the plotted potential range. The dashed lines correspond to linear fits to the data.

surface to 395 meV in the water-covered case. As a consequence, the reduction of the atomic binding energies is compensated by the increase in the barrier height, so that the difference, which is the barrier for hydrogen desorption, remains almost unchanged [30].

The dependence of the barrier for the Tafel reaction on the potential is approximately linear. The slope of the linear fit to the data,

$$\alpha = \frac{dE_a}{d\phi}, \quad (20)$$

gives the so-called transfer coefficient which is a measure of the symmetry of the activation barrier. The value of  $\alpha = 0.64$  for the Tafel reaction indicates that the barrier location for the Tafel reaction is closer to the initial state at the electrode, whereas  $\alpha = 0.42$  for the Heyrovsky mechanism means that in this case the barrier is closer to the outer Helmholtz plane.

At potentials around 0 V, the hydrogen coverage becomes 1, and further hydrogen adsorption only occurs at potentials below  $-0.5$  V. At negative potentials where hydrogen evolution becomes thermodynamically possible, both the Tafel and the Heyrovsky reaction exhibit moderate barriers. Figure 20 demonstrates that the calculated barriers for the Heyrovsky mechanism are smaller than for the Tafel mechanism. This suggests that the Heyrovsky reaction dominates the hydrogen evolution. Experimentally, the mechanism for the hydrogen evolution on Pt electrodes has been found to depend on the electrode orientation [49]. As for Pt(111), the exact reaction mechanism could not be unambiguously deduced, the measured activation energy of 0.18 eV [49], however, is smaller than those calculated in the DFT study [10].

This indicates that an even more realistic description of the hydrogen evolution on Pt electrodes might be required.

## V. CONCLUSIONS

This brief review has demonstrated that periodic density functional theory calculations can be quite powerful in elucidating details of the metal/water interface in the absence and the presence of external fields from first principles. Because of the still incomplete status of our knowledge about the microscopic nature of struc-

tures and processes at the electrochemical solid/liquid interface, there are many open questions remaining which wait to be addressed by theory. However, the theoretical description of the solid/liquid interface in the presence of varying electrode potentials is not trivial. It is certainly fair to say that the first-principles treatment of these systems has not matured yet. Several different theoretical approaches to represent external fields and varying electrode potentials exist, and all have advantages and disadvantages. There is still room for improvements in the realistic theoretical description of electrochemical solid-liquid interfaces. This makes this research field demanding, but also exciting.

- 
- [1] G. Ertl, *Angew. Chem. Int. Ed.* **47**, 3524 (2008).  
 [2] A. Groß, *Surf. Sci.* **500**, 347 (2002).  
 [3] W. Kohn, *Rev. Mod. Phys.* **71**, 1253 (1999).  
 [4] F. Besenbacher, I. Chorkendorff, B. S. Clausen, B. Hammer, A. M. Molenbroek, J. K. Nørskov, and I. Stensgaard, *Science* **279**, 1913 (1998).  
 [5] N. M. Marković and P. N. Ross Jr., *Surf. Sci. Rep.* **45**, 117 (2002).  
 [6] A. Y. Lozovoi, A. Alavi, J. Kohanoff, and R. M. Lynden-Bell, *J. Chem. Phys.* **115**, 1661 (2001).  
 [7] A. Roudgar and A. Groß, *Chem. Phys. Lett.* **409**, 157 (2005).  
 [8] J. S. Filhol and M. Neurock, *Angew. Chem. Int. Ed.* **45**, 402 (2006).  
 [9] C. D. Taylor, S. A. Wasileski, J.-S. Filhol, and M. Neurock, *Phys. Rev. B* **73**, 165402 (2006).  
 [10] E. Skúlason, G. S. Karlberg, J. Rossmeisl, T. Bligaard, J. Greeley, H. Jónsson, and J. K. Nørskov, *Phys. Chem. Chem. Phys.* **9**, 3241 (2007).  
 [11] W. Schmickler, *Chem. Rev.* **96**, 3177 (1996).  
 [12] J. I. Siepmann and M. Sprik, *J. Chem. Phys.* **102**, 511 (1995).  
 [13] R. Bukowski, K. Szalewicz, G. C. Groenenboom, and A. van der Avoird, *Science* **315**, 1249 (2007).  
 [14] A. Michaelides, *Appl. Phys. A* **85**, 415 (2006).  
 [15] G. Kresse and J. Furthmüller, *Phys. Rev. B* **54**, 11169 (1996).  
 [16] J. P. Perdew, K. Burke, and M. Ernzerhof, *Phys. Rev. Lett.* **77**, 3865 (1996).  
 [17] B. Hammer, L. B. Hansen, and J. K. Nørskov, *Phys. Rev. B* **59**, 7413 (1999).  
 [18] J. Neugebauer and M. Scheffler, *Phys. Rev. B* **46**, 16067 (1992).  
 [19] N. D. Mermin, *Phys. Rev.* **137**, A 1441 (1965).  
 [20] A. Alavi, J. Kohanoff, M. Parrinello, and D. Frenkel, *Phys. Rev. Lett.* **73**, 2599 (1994).  
 [21] S. A. Wasileski and M. J. Janik, *Phys. Chem. Chem. Phys.* **10**, 3613 (2008).  
 [22] N. W. Ashcroft and N. D. Mermin, *Solid State Physics* (Saunders College, Philadelphia, 1976).  
 [23] C. L. Fu and K. M. Ho, *Phys. Rev. Lett.* **63**, 1617 (1989).  
 [24] K. P. Bohnen and D. M. Kolb, *Surf. Sci.* **407**, L629 (1998), ISSN 0039-6028, potential dependence.  
 [25] A. Y. Lozovoi and A. Alavi, *Phys. Rev. B* **68**, 245416 (2003).  
 [26] P. A. Thiel and T. E. Madey, *Surf. Sci. Rep.* **7**, 211 (1987).  
 [27] M. A. Henderson, *Surf. Sci. Rep.* **46**, 1 (2002).  
 [28] A. Roudgar and A. Groß, *Surf. Sci.* **597**, 42 (2005).  
 [29] P. J. Feibelman, *Science* **295**, 99 (2002).  
 [30] Y. Gohda, S. Schnur, and A. Groß, *Faraday Discuss.* **140**, 233 (2009).  
 [31] A. Michaelides, V. A. Ranea, P. L. de Andres, and D. A. King, *Phys. Rev. Lett.* **90**, 216102 (2003).  
 [32] J. S. Filhol and M.-L. Bocquet, *Chem. Phys. Lett.* **238**, 203 (2007).  
 [33] S. Izvekov and G. A. Voth, *J. Chem. Phys.* **115**, 7196 (2001).  
 [34] R. Car and M. Parrinello, *Phys. Rev. Lett.* **55**, 2471 (1985).  
 [35] H. Noguchi, T. Okada, and K. Uosaki, *Faraday Discuss.* **140**, 125 (2009).  
 [36] S. Ye, S. Nihonyanagi, and K. Uosaki, *Phys. Chem. Chem. Phys.* **3**, 3463 (2001).  
 [37] M. Schmitz and P. Tavan, *J. Chem. Phys.* **121**, 12247 (2004).  
 [38] A. Roudgar and A. Groß, *J. Electroanal. Chem.* **548**, 121 (2003).  
 [39] M. F. Toney, J. N. Howard, J. Richer, G. L. Borges, J. G. Gordon, O. R. Melroy, D. G. Wiesler, D. Yee, and L. B. Sorensen, *Nature* **368**, 444 (1994).  
 [40] M. F. Toney, J. N. Howard, J. Richer, G. L. Borges, J. G. Gordon, O. R. Melroy, D. G. Wiesler, D. Yee, and L. B. Sorensen, *Surf. Sci.* **335**, 326 (1995).  
 [41] K. Morgenstern and J. Nieminen, *J. Chem. Phys.* **120**, 10786 (2004).  
 [42] O. Sugino, I. Hamada, M. Otani, Y. Morikawa, T. Ikeshoji, and Y. Okamoto, *Surf. Sci.* **601**, 5237 (2007).  
 [43] M. Otani, I. Hamada, O. Sugino, Y. Morikawa, Y. Okamoto, and T. Ikeshoji, *Phys. Chem. Chem. Phys.* **10**, 3609 (2008).  
 [44] M. Otani and O. Sugino, *Phys. Rev. B* **73**, 115407 (2006).  
 [45] G. A. Kimmel, N. G. Petrik, Z. Dohnálek, and B. D. Kay, *Phys. Rev. Lett.* **95**, 166102 (2005).  
 [46] G. Henkelman and H. Jónsson, *J. Chem. Phys.* **113**, 9978 (2000).  
 [47] G. Henkelman, B. P. Uberuaga, and H. Jónsson, *J. Chem. Phys.* **113**, 9901 (2000).  
 [48] J. Rossmeisl, E. Skúlason, M. J. Björketun, V. Tripkovic, and J. K. Nørskov, *Chem. Phys. Lett.* **466**, 68 (2008).

- [49] N. M. Marković, B. N. Grgur, and P. N. Ross, *J. Phys. Chem. B* **101**, 5405 (1997).